Nano Research 2018, 11(1): 586–602
https://doi.org/10.1007/s12274-017-1834-6
Research Article
ISSN 1998-0124
CN 11-5974/O4

Cross-linked self-assembling peptide scaffolds

Raffaele Pugliese[1], Amanda Marchini[1,2], Gloria Anna Ada Saracino[2], Ronald N. Zuckermann[3], and Fabrizio Gelain[1,2] (✉)

[1] *IRCCS Casa Sollievo della Sofferenza, Opera di San Pio da Pietralcina, Viale Capuccini 1 San Giovanni Rotondo, Foggia 71013, Italy*
[2] *Center for Nanomedicine and Tissue Engineering (CNTE), A. O. Ospedale Niguarda Cà Granda, Piazza dell' Ospedale Maggiore 3, Milan 20162, Italy*
[3] *The Molecular Foundry, Lawrence Berkeley National Laboratory, 1 Cyclotron Road, Berkeley, California 94720, USA*

Received: 23 February 2017
Revised: 30 August 2017
Accepted: 31 August 2017

KEYWORDS
self-assembling peptide, co-assembling peptide, cross-linking, sulfo-SMCC, supramolecular self-assembly

ABSTRACT

Self-assembling peptides (SAPs) are synthetic bioinspired biomaterials that can be feasibly multi-functionalized for cell transplantation and/or drug delivery therapies. Despite their superior biocompatibility and ease of scaling-up for production, they are unfortunately hampered by weak mechanical properties due to transient non-covalent interactions among and within the self-assembled peptide chains, thus limiting their potential applications as fillers, hemostat solutions, and fragile scaffolds for soft tissues. Here, we have developed and characterized a cross-linking strategy that increases both the stiffness and the tailorability of SAP hydrogels, enabling the preparation of transparent flexible threads, discs, channels, and hemispherical constructs. Empirical and computational results, in close agreement with each other, confirmed that the cross-linking reaction does not affect the previously self-assembled secondary structures. *In vitro* tests also provided a first hint of satisfactory biocompatibility by favoring viability and differentiation of human neural stem cells. This work could bring self-assembling peptide technology to many applications that have been precluded so far, especially in regenerative medicine.

1 Introduction

Self-assembling and co-assembling peptides (SAPs and CAPs) have attracted increasing interest in the scientific community as tailorable, synthetic, and biocompatible biomaterials for regenerative medicine applications [1, 2]. They have been used as hemostat solutions [3], bone fillers [4], wound healers [5, 6], and as injectable scaffolds for the regeneration of infarcted heart, degenerated cartilage, and injured nucleus pulposus [7–12]. In addition, a few clinical trials are currently assessing their potential for remineralization in dental repair [13]. In the field of neural tissue engineering, SAPs have shown intriguing potential in the treatment of brain injuries [14, 15], spinal cord injuries [10, 16, 17], and Alzheimer's disease [18, 19]. Here, SAP biomaterials were tested as self-adapting scaffolds to prevent hemorrhage and

Address correspondence to f.gelain@css-mendel.it

decrease harmful immune responses (in the case of acute injuries), as injectable scaffolds capable of spatially guiding the regenerating nervous tissue and creating suitable microenvironments for nervous regeneration. In the case of Alzheimer's disease, they significantly improved cognitive impairment by interfering with Aβ plaque formation.

SAPs mimic the natural peptide-based extracellular matrix (ECM), and also display multiple, specific functional motifs that interact with cells [20] and proteins [21] (if designed to do so); furthermore, self-assembly usually takes place at physiological pH and osmolarity. Furthermore, SAPs and CAPs are synthetic, pathogen-free, and mainly used at low concentrations in water (less than 8%, w/v), all of which are desirable properties for potentially effective therapies in the future. Despite these promising results, several other tissue engineering applications are precluded, because of the poor mechanical stability of these materials due to the non-covalent nature of their supramolecular assemblies [22]. Indeed, these assemblies interact only through weak, non-covalent interactions such as electrostatic attractions, H-bonds, van der Waal's (VDW) forces, and hydrophobic forces. Thus, fragile and soft SAP scaffolds have been used mainly for soft tissue regeneration or as fillers, but their use has been precluded in several other tissue engineering applications. Taking inspiration from the use of cross-linked proteins such as collagen and silk fibroin in tissue engineering [23–25], we used sulfo-SMCC, an amine-to-sulfhydryl cross-linker that contains N-hydroxysuccinimide (NHS) ester and maleimide reactive groups at opposite ends, to further stabilize the self-assembled hydrogels of the Ac-CGGLKLKL KLKLKLKGGC-$CONH_2$ peptide (named CK). Sulfo-SMCC is already being used in the manufacturing protocol of a new oxygen transport agent in an approved and ongoing multi-center clinical trial [26–28]; thus, the translational potential of its usage for other therapies is promising. In our case, we observed an increase of two orders of magnitude in both stiffness and failure stress, in comparison with standard fragile SAP hydrogels. This enhancement allowed us to obtain flexible threads, discs, and microchannels made entirely of cross-linked CK peptide (crossCK), which have never been obtained before. The good agreement between the deep empirical characterization data and molecular modeling analyses suggested that cross-linking fastens the pre-existing self-assembled aggregates without significantly altering their secondary structures, thus potentially allowing functionalization (and other strategies developed so far in decades of research in the field of SAPs) to be used in cross-linked SAPs. Despite the chemical modification of the assembled scaffolds, biocompatibility with human neural stem cells (hNSCs) was demonstrated by *in vitro* experiments, in which satisfactory viability and differentiation were achieved. Lastly, we foresee that by cross-linking SAPs, it will eventually be possible to develop functionalized synthetic scaffolds with tunable bioabsorption times and/or bioactivities suitable for use in blood vessels, heart patches, corneal replacement, and even bioabsorbable sutures for surgeries.

2 Experimental

2.1 Peptide synthesis and purification

CK peptide was synthetized on Rink amide 4-methylbenzhydrylamine resin (0.5 $mmol \cdot g^{-1}$ substitution) using the Liberty-Discovery (CEM) microwave automated synthesizer. The peptide was cleaved from the resin by addition of TFA:H_2O:EDT:TIS (94:2.5:2.5:1). Raw peptide was precipitated using cold ethyl ether and then lyophilized (Labconco). The resulting raw peptide was purified using a Waters binary high-performance liquid chromatography (HPLC) apparatus (> 95%). For all the experiments, the peptide powder was dissolved to a final concentration of 5% (w/v) in distilled water (Gibco).

2.2 Cross-linking reaction

CrossCK was prepared by adding 0.45, 0.91, 2.7, 5.4, 10, or 15 mM of sulfo-SMCC dissolved in 1 mL of DPBS:H_2O (1:1, v/v) to 20 mM of CK peptide dissolved in 100 μL of distilled water. The cross-linking solution and crossCK were incubated overnight at room temperature. At the end of the reaction, the unreacted sulfo-SMCC in the supernatant was removed by aspiration with a vacuum pipette, and the resulting crossCK was washed and suspended in 1.5 mL of DPBS for 1 h. Washes were repeated 5 times before use.

2.3 Ellman's reagent assay

The cross-linking degree of crossCK hydrogels was assessed using Ellman's reagent (5,5′-dithio-bis(2-nitrobenzoic acid); also known as DTNB) (Thermo Scientific), which is a water-soluble compound for quantitating free sulfhydryl (SH–) groups in peptides and proteins. SH-groups were quantized based on molar absorptivity using the extinction coefficient of TNB (14,150 $M^{-1}\cdot cm^{-1}$) at 412 nm as reference [29, 30]. Further details are provided in the Electronic Supplementary Material (ESM).

2.4 Fourier transform infrared spectroscopy (FTIR) analysis

FTIR analysis of assembled nanostructures was performed on CK peptide dissolved at a concentration of 5% (w/v) in distilled water, and on crossCK film, after 24 h incubation at 4 ˚C. FTIR spectra were recorded in attenuated total reflection (ATR) using a Perkin Elmer Spectrum 100 spectrometer. Each sample was analyzed in triplicate.

2.5 Raman analysis

Cross-linking identification and stability analysis of the assembled crossCK nanostructure were carried out using confocal Raman microscopy (LabRAM Aramis, Horiba Jobin Yvon). Raman spectra were acquired from dried samples through water evaporation. The conditions employed to collect spectra were a 50 long-working distance (LWD) objective (numerical aperture 0.55) and a 785 nm laser wavelength. The confocal pinhole was opened to 200 μm, and the depth of focus was 1–10 μm. Each analysis was carried out in triplicate.

2.6 X-ray diffraction (XRD) analysis

XRD patterns were collected using a multiple-wavelength anomalous diffraction and monochromatic macromolecular crystallography beamline (8.3.1) located at the Advanced Light Source (ALS), Lawrence Berkeley National Laboratory, as previously described [31].

2.7 Wide-angle X-ray scattering (WAXS)

WAXS data were collected at the ALS beamline 7.3.3 (Lawrence Berkeley National Laboratory) with a multilayer monochromator. The X-ray scattering pattern was recorded with an ADSC Quantum 4r CCD detector that was positioned ~ 1,000 mm from the samples. The beamline is designed to be operated at 10 keV [32].

2.8 Atomic force microscopy (AFM) analysis

AFM images were captured in tapping mode by a Multimode Nanoscope V (Digital Instruments, Veeco), using single-beam silicon cantilever probes (Veeco RFESP MPP-21100–10, cantilever f0, 59–69 kHz; constant force: 3 $N\cdot m^{-1}$). Peptides were dissolved in distilled water at a concentration of 5% (w/v) and sonicated for 20 min, the same day as imaging. After sonication, the cross-linking reaction of the crossCK took place. 100 different nanofibers on approximately 10 independent fields per sample were measured, and characterized as previously described [33].

2.9 Rheological tests

Rheological properties of the CK and crossCK hydrogels were investigated with an AR-2000ex rheometer (TA Instruments). A truncated cone-plate geometry (acrylic truncated diameter 20 mm; truncation 34 μm; angle 1%) was used. All measurements were obtained at 25 ˚C using a Peltier cell as the lower plate of the instrument to control the temperature during each test. Each experiment was performed in triplicate.

2.10 Molecular dynamics simulations

All-trans conformations of CK peptides were generated with PyMOL (http://www.pymol.org), and 300 peptides were randomly distributed in cubic boxes with a 32 nm edge to simulate the concentration used in empirical experiments (5%, w/v). Atoms belonging to different peptides were at minimum distances of 10 Å from each other. The systems were translated into a coarse-grained (CG) model consistent with version 2.2 of the MARTINI force field [34, 35]. Molecular dynamics simulations were performed using version 4.5.5 of the GROMACS package [36].

2.11 hNSC viability, proliferation and differentiation assays

hNSCs were obtained according to good manufacturing

practice protocols, in agreement with the guidelines of the European Medicines Agency (EMA) and Agenzia Italiana del Farmaco (AIFA) [37]. hNSC were expanded as previously described [38].

All data were processed using GraphPad Prism 7 software. The MTT assay was evaluated through one-way ANOVA followed by Tukey's multiple comparison test; four independent experiments were performed. Results of neuronal and astroglial cell differentiation were analyzed by two-way ANOVA and Bonferroni post-test, while oligodendrocyte differentiation was analyzed by one-way ANOVA followed by Tukey's comparison test. Values of $p < 0.05$ were considered statistically significant. Three independent experiments were performed per test.

3 Results and discussion

3.1 Design of cross-linking reaction and scaffold production

RADA16-I and LDLK12 are widely studied and well-characterized SAPs in the field of regenerative medicine [39]. Their total net charge is around zero at neutral pH, and they can be feasibly functionalized with short epitopes at both termini to obtain biomimetic scaffolds customized for specific applications [2]. However, in longer peptide chains, as expected in the case of extensive cross-linking, hydrophobic packing may cause issues of solubility if it is not counter-balanced by sufficient electrostatic charge repulsion. We previously demonstrated that the highly charged peptide LKLK12 can both weakly self-assemble at neutral pH and strongly co-assemble with the oppositely charged peptide LDLD12 [38]. Also, both peptides can be functionalized at both ends. In all cases, we provided the amino and SH-groups necessary for sulfo-SMCC cross-linking by functionalizing LKLK12 with cysteines at both ends, spaced by two glycines each, yielding the CK peptide. Peptide capping was preferred in order to preserve stability over time. Upon pH shift (from acid to basic), water solutions of CK (at 5%, w/v) spontaneously formed a fragile hydrogel scaffold similar to those of RADA16-I and LDLK12 [39], with very limited flexibility and processing potential. Conversely, applying the cross-linking reaction described in Section 2.2 to same-concentration solutions of CK, we obtained scaffolds made of crossCK that displayed a remarkable improvement in resilience and processability. Indeed, we managed to cross-link extruded threads (Fig. 1(a)) to obtain flexible constructs (Figs. 1(a1)–1(a4)) and

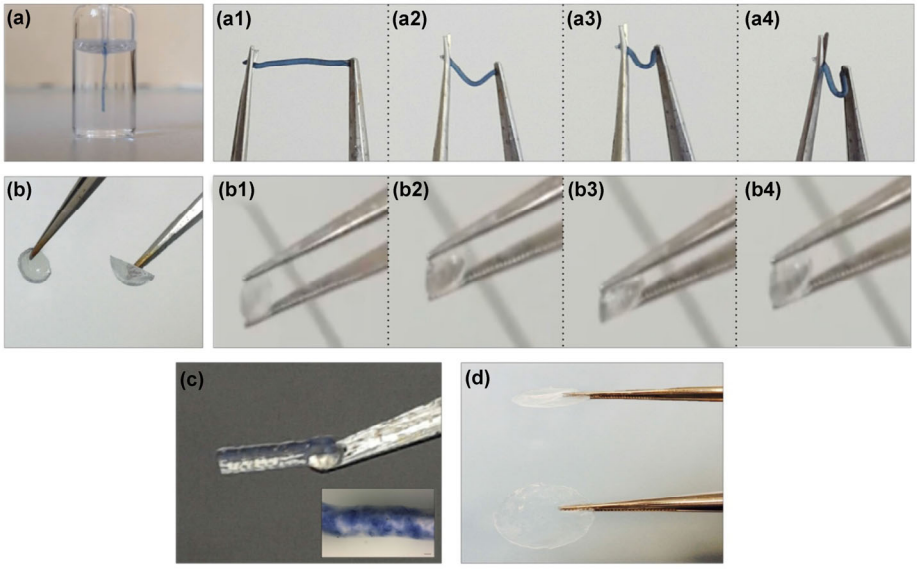

Figure 1 Examples of scaffolds made of the crossCK peptide. (a) Threads can be extruded into a cross-linking solution; After reaction, they display a high degree of flexibility ((a1)–(a4)). (b) Hemispherical constructs are resilient to compression ((b1)–(b4)). (c) Hollow microchannels are obtained via a coaxial needle fed by a syringe pump. (d) Flat discs are cast on a disposable insert. All cross-linked scaffolds are transparent; trypan blue was added to improve scaffold visualization.

Video S1 in the ESM). We produced hemispherical constructs resilient to compression (Fig. 1(b) and Video S2 in the ESM), hollow microchannels (Fig. 1(c)), and flat discs (Fig. 1(d)) entirely made of crossCK. All scaffolds were transparent (a synthetic dye was added to improve scaffold localization). Keeping in mind that other scaffold shapes could be feasibly obtained, to the best of our knowledge, this is the first report of such diverse flexible scaffolds entirely made of peptides.

3.2 Biomechanical characterization

Since scaffold mechanical properties should be tuned to match the mechanical properties of the target tissue to be regenerated, biomechanical characterization of crossCK scaffolds was crucial to assess whether they were still soft constructs or had become stiffer scaffolds, thus enlarging their range of potential applications. In the case of hydrogels, the most relevant characteristics are the storage modulus (G') and loss modulus (G''), which can be measured by a rheometer. An increase in G' as a function of time can be indicative of ongoing structural and networking processes [40]. Usually, in β-sheet-rich SAPs after self-assembly, interactions among self-assembled fibers lead to the formation of an entangled nanofibrous network and increased values of G' [8]. The ratio between G' and G'' provides insights into the viscoelastic properties of the tested scaffold, i.e., whether it behaves as a viscous liquid ($G' < G''$) or as an elastic solid ($G' > G''$) [2].

By monitoring the temporal evolution of G' and G'', we observed the gelation kinetics and the increasing hydrogel stiffness of both CK and crossCK peptides with 10 mM of sulfo-SMCC (Fig. 2(a)). Liquid solutions were monitored via time-sweep tests for 15 h after exposure to a sulfo-SMCC cross-linker (for crossCK only) and pH shift. The pH shift is the external stimulus triggering both self-assembly and cross-linking (see section 3.1 for details). Gelation kinetics and increasing hydrogel stiffness were also observed for crossCK with sulfo-SMCC concentrations of 0.45, 0.91, 2.7, 5.4, and 15 mM (Fig. S1 in the ESM). Trends of G' and G'' for all peptides showed typical hydrogel-like profiles, featuring a predominant elastic solid-like behavior (G'), as compared with the viscous component (G''). CK displayed an average G' value of 5 kPa, which is typical of soft hydrogels made of SAPs [10]. By contrast, the crossCK peptides showed an increase in stiffness depending on the sulfo-SMCC concentration. This ranged from ~ 6 kPa (with 0.45 mM sulfo-SMCC) to ~ 140 kPa (with 15 mM sulfo-SMCC), reaching a remarkable G' value of 170 kPa at 10 mM of sulfo-SMCC.

In the latter case, cross-linking led to an increase in stiffness of two orders of magnitude, resulting in a scaffold with as-yet-unmatched G' values for an SAP hydrogel. This notable increase in the storage modulus was likely due to the formation of covalent cross-links concomitant with self-assembly, that is, two spontaneous phenomena activated by the pH shift.

Similar results in terms of storage modulus were obtained with a Fmoc-linked peptide (in dimethyl sulfoxide) and a lauryl-amphiphilic peptide, through photo-cross-linking and reaction with glutaraldehyde, respectively [41, 42]. However, the use of unnatural residues and toxic solvents may limit the translational potential of these strategies in humans.

In subsequent frequency-sweep tests (Fig. 2(a1) and Fig. S1(a) in the ESM), the G' and G'' profiles were almost unchanged along the tested frequency range (0.1–1,000 Hz), displaying a solid-like behavior for both peptides ($G' > G''$), but maintaining far higher average G' and G'' values for crossCK (Fig. 2(a2) and Fig. S1(a1) in the ESM). Failure stress tests were performed within the linear viscoelasticity region to assess material failure when subjected to a linear stress/strain progression at +25 °C. While failure occurred for a stress of more than 3,000 Pa for crossCK (10 mM sulfo-SMCC) (Fig. 2(b)), this was not the case for CK, which failed at ~ 55 Pa (Fig. 2(b1)); this two-orders-of-magnitude difference between crossCK and CK (Fig. 2(b2)) can be attributed to the efficient formation of chemical cross-links in addition to the standard weak intermolecular interactions present in soft self-assembled hydrogels. An increase in failure stress was also observed in the crossCK peptides for 0.45, 0.91, 2.7, 5.4, and 15 mM of sulfo-SMCC, with failure occurring at stresses of ~ 20, 137, 1,594, 2,400, and 2,711 Pa, respectively (Figs. S1(b)–S1(b2) in the ESM). Last, the viscosity (μ) of hydrogels, an estimate of the degree of entanglement and network formation, was measured as a function of shear rate (Fig. 2(c)). With

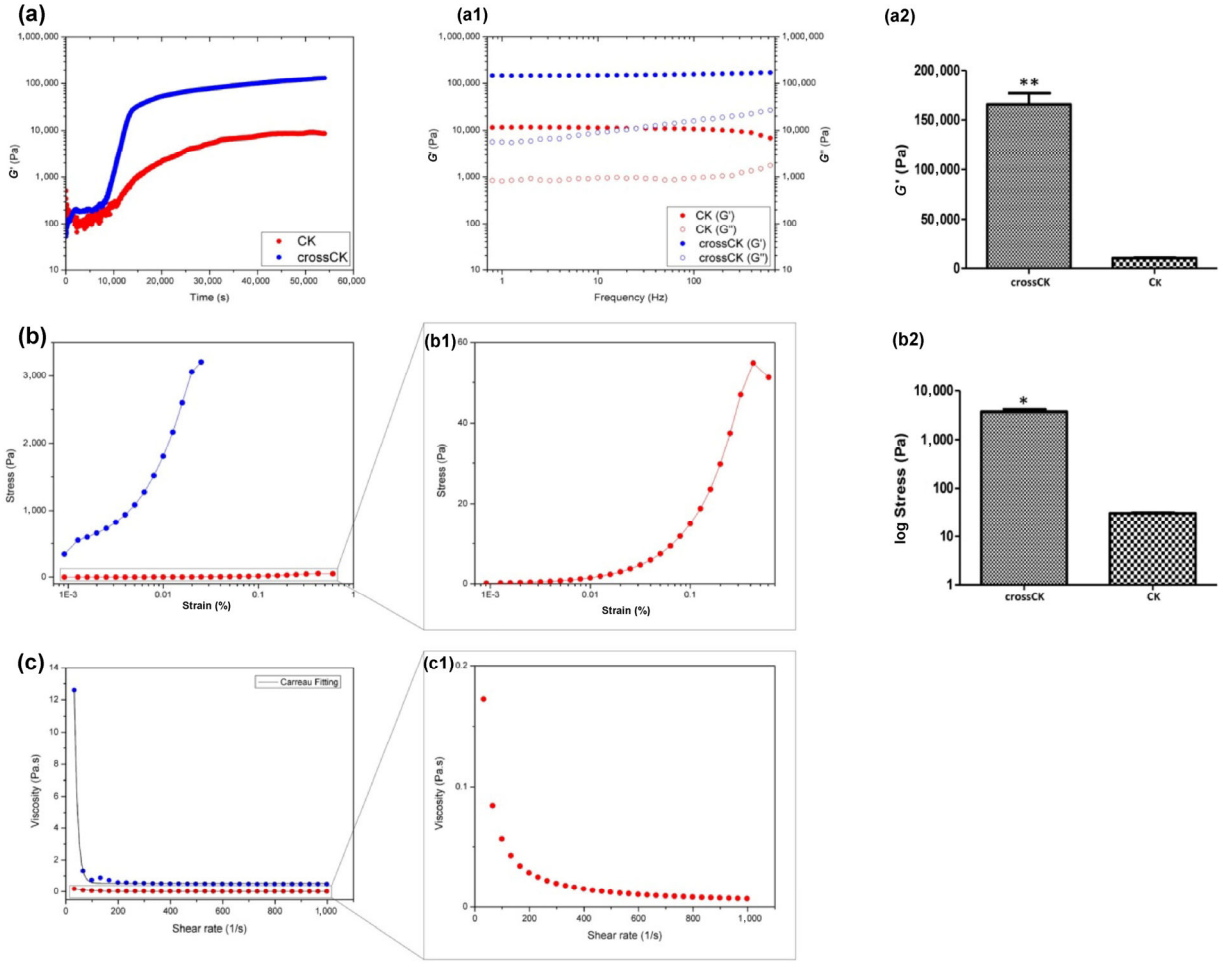

Figure 2 Rheological characterization of the CK and crossCK hydrogels. Peptide solutions were monitored via a 15 h time-sweep test (a) immediately after initiation of self-assembly and the cross-linking reaction (for crossCK only), followed by a frequency sweep test (0.1–1,000 Hz) (a1). The typical hydrogel profile was confirmed for both peptides, displaying a predominant solid-like behavior (G′) (solid dots) compared with the viscous component (G″) (empty dots). While the CK peptide had a G′ value of 5 kPa (in red), similar to a weak hydrogel, crossCK reached a G′ value of 170 kPa (in blue), revealing a solid-elastic behavior. The cross-linking led to a significant increase in the stiffness (of two orders of magnitude) compared with the CK peptide (a2) (n = 3). In strain-stress failure tests ((b) and (b1)), crossCK showed a substantial failure stress increase compared with CK (n = 3) (b2), likely as a result of additional covalent interactions that hold up the crossCK self-assembled nanostructures. The viscosity profiles of assembled CK and crossCK peptides were measured as a function of continuous shear rate ramps ((c) and (c1)). Both peptides showed typical trends of non-Newtonian fluids, but crossCK exhibited higher viscosity values than CK, confirming a relationship between the viscosity and degree of network formation. Obtained experimental viscosities were fitted with the Carreau equation (black lines).

increasing shear rate values, both peptides showed a viscosity decrease typical of non-Newtonian fluids. Nonetheless, the higher μ values for crossCK (Figs. 2(c) and 2(c1)) provided evidence of real cross-linking and over-structuring.

In summary, crossCK scaffolds displayed an unmatched improvement in both stiffness and failure stress, which was likely a result of the cross-linking reaction.

3.3 Effective cross-linking and its influence on assembled secondary structures

To evaluate the reaction kinetics and the degree of cross-linking on the assembled hydrogels, Ellman's reagent was used to quantitatively measure the free SH-groups during the cross-linking reaction. This compound is based on the reaction of thiol with DTNB, upon which a mixed disulfide (R-S-TNB) and one

equivalent of TNB^{2-} are formed. The latter produces a measurable yellow-colored product when it reacts with SH-groups, exhibiting intense light absorption at 412 nm [43]. As expected, CK did not show changes over time in its percentage of free SH-groups, while crossCK displayed a decrease during the time course of the reaction (Fig. 3). At low concentrations of sulfo-SMCC, the reaction kinetics were slow; free thiol values of 47%, 44.6%, and 38% were reached after 24 h, with 0.45, 0.91, and 2.7 mM of sulfo-SMCC, respectively. However, relatively fast reactions were observed with 5.4 and 10 mM of sulfo-SMCC, reaching 28% and 19% free SH-groups after 24 h, respectively. This spectrophotometric measurement provided an indirect insight into the yield of the cross-linking reaction, highlighting its timing and how strongly it is influenced by sulfo-SMCC concentration.

The extent of the cross-linking reaction and its influence on the secondary structure of CK was assessed by Raman spectroscopy. Raman spectra of both CK and crossCK peptides revealed vibrational

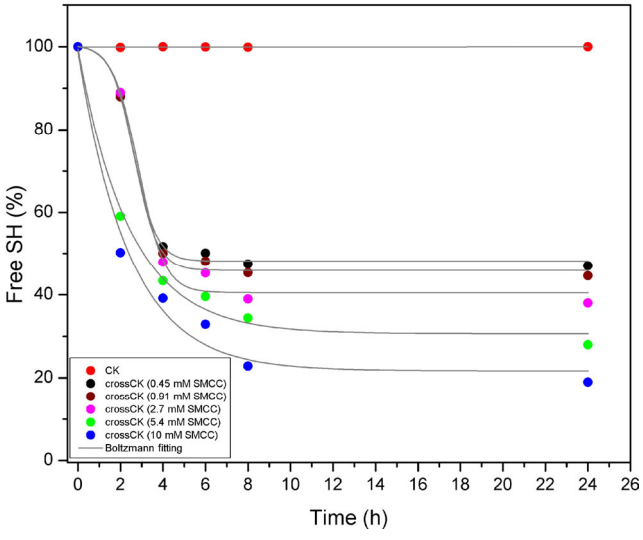

Figure 3 Reaction kinetics of DTNB with the free thiol in CK and crossCK peptides. Peptide solutions were monitored by spectrophotometric thiol assay for 24 h. While CK peptide (in red) did not display changes in free SH-groups, crossCK peptides showed a decrease in free SH-groups during the time course of the reaction, depending on the sulfo-SMCC concentration. At 24 h, crossCK with 0.45 mM (in black), 0.91 mM (in amaranth), and 2.7 mM (in magenta) of sulfo-SMCC showed free-thiol values of 47%, 44.6%, and 38%, respectively. By contrast, crossCK at 5.4 mM (in green) and 10 mM (in blue) of sulfo-SMCC reached free-thiol values of 28% and 19%, respectively.

peaks found in β-sheet structures (Fig. 4(a)), i.e., a broad band at 1,650 cm^{-1} (amide I region) associated with C=O stretching in β-sheets, and a narrow band at 1,550 cm^{-1} (amide II region) associated with both NH bending (60%) and CN stretching (40%) in parallel/anti-parallel β-sheet structures [33, 44].

CrossCK showed a further band at approximately 1,766 cm^{-1}, due to the symmetric stretching of imide moieties of sulfo-SMCC [45]. A fully-quenched sulfo-SMCC (see ESM for details) was incubated with CK to determine whether the vibrational peak at 1,766 cm^{-1} (which was also detected in the fully-quenched sulfo-SMCC) indicated an effective linking of sulfo-SMCC to CK, or whether it might be ascribable to unreacted sulfo-SMCC molecules as well.

Only vibrational peaks in the amide I and amide II regions were observed, suggesting that only reactive sulfo-SMCC effectively integrated within the final cross-linked nanostructures, presumably by means of its NHS-ester and maleimide groups reacting with the lysines and cysteines of the CK. No signal ascribable to sulfo-SMCC was observed, leading us to suppose that the amount of unbound sulfo-SMCC, if present, was below the detection threshold. Therefore, after the cross-linking reaction, residues of the cross-linker may be efficiently removed.

The cross-linking reaction was also assessed via tricine-sodium dodecyl sulfate-polyacrylamide gel electrophoresis (tricine-SDS-PAGE) and matrix assisted laser desorption ionization-time of flight (MALDI-TOF) analysis to follow the increase of the molecular weight of crossCK molecules over time. Tricine-SDS-PAGE [46] (10%–16% gel) analysis of the reaction with 10 mM sulfo-SMCC showed cross-linked adducts (molecular weight ~ 4.6 kDa) after 1 h of the cross-linking reaction (Fig. S2 in the ESM); dimer formation was confirmed through MALDI-TOF analysis (Fig. S3 in the ESM). Higher-molecular-weight bands (7–10 kDa) appeared after 2 h of reaction, overlapped by a smeared signal, likely indicating the presence of a heterogeneous population of higher-molecular-weight molecules formed by extensive cross-linking. For longer time frames, no band was observed to enter the gel, likely owing to a rapid increase in the degree of cross-linking and, as a consequence, the formation of complex

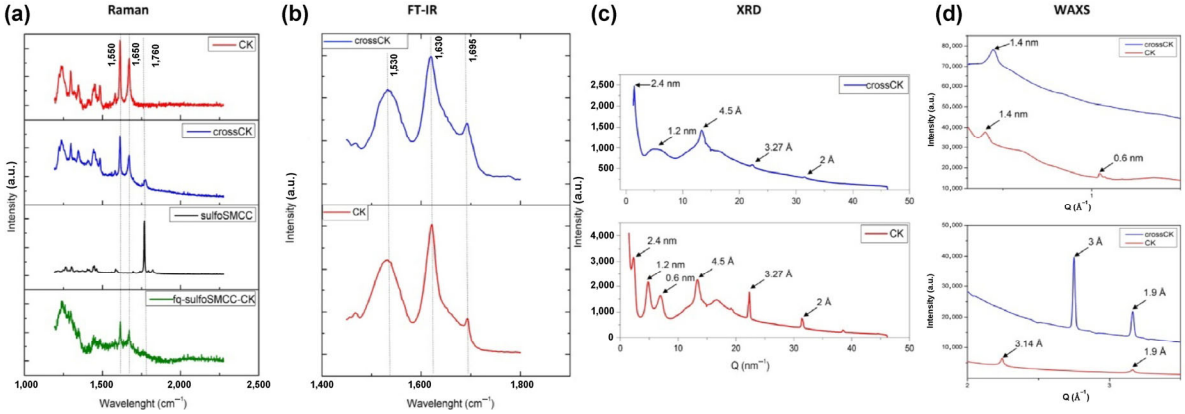

Figure 4 Structural characterization of assembled scaffolds. (a) Raman spectra (1,000–2,500 cm^{-1} region) of CK (red), crossCK (blue), sulfo-SMCC (black), and fully-quenched sulfo-SMCC-CK (green). Both CK and crossCK peptides showed typical features of β-sheet structures, such as a broad band at 1,650 cm^{-1} (amide I region) and a narrow band at 1,550 cm^{-1} (amide II region). The vibrational peak at 1,766 cm^{-1} in the crossCK spectrum is likely to be due to the symmetric stretching of imide moieties of sulfo-SMCC, suggesting the presence of covalent linking between amide and sulfhydryl groups. When using fully quenched sulfo-SMCC and CK, the amide I and amide II components were detected, but with no relevant contribution of unbound sulfo-SMCC moieties. (b) ATR-FTIR spectra in the amide I and amide II absorption regions of CK and crossCK. Both peptides' spectra displayed a broad band at 1,530 cm^{-1} (amide II region), which is indicative of β-sheet aggregation; in addition, peaks at 1,630 and 1,695 cm^{-1} (amide I region) suggest the presence of antiparallel β-sheet structures. (c) XRD analysis demonstrated that both CK and crossCK show similar X-ray patterns. The most significant peaks were identified at 4.5 Å and 2.4 nm, indicating a predominant β-sheet secondary structure and the presence of double layers of β-sheets, respectively. The 1.2 nm spacing can be interpreted as the distance between two layers of β-sheets. The 3.27 Å spacing is ascribed to the distance between each residue along the peptide chain. The peak at 2 Å is considered the second order of the 4.5 Å peak. The 0.6 nm spacing is related to the lysine side-chain length; its absence in crossCK is probably due to the linking of lysines with imide moieties. (d) WAXS data confirmed the propensity of both peptides to form β-structures, owing to the presence of peaks at 1.9 Å, ~3 Å, and ~1.4 nm.

molecular networks hampering the mobility of the sample through the gel.

Further structural characterization of CK and crossCK peptides was performed using ATR-FTIR. In the amide II region (1,480–1,575 cm^{-1}) of the FTIR spectra of both CK and crossCK, aggregation was suggested by the presence of a peak at 1,530 cm^{-1}, indicative of CN stretching and NH bending in β-sheets (Fig. 4(b)). With FTIR spectroscopy, the ratio of parallel/antiparallel β-sheet structures can be quantified by assessing the vibrational peaks within the amide I region (1,600–1,700 cm^{-1}) [47]. Briefly, Sarroukh et al. suggested that the β-sheet organizational index ($I_{1,695}/I_{1,630}$), the ratio of peak intensities at 1,695 cm^{-1} (present in antiparallel sheets only) and 1,630 cm^{-1}, is proportional to the ratio of antiparallel/parallel β-sheet structures [48]. In both CK and crossCK, the β-sheet organizational index was ~ 30%, suggesting the presence of anti-parallel β-sheets in both peptides. Moreover, the bands observed at 1,530, 1,630, and 1,695 cm^{-1}, assigned to β-sheet formation, were found also in the crossCK with 0.45, 0.91, 2.7, 5.4, and 15 mM sulfo-SMCC solutions (Fig. S4 in the ESM), with a slight variation of the β-sheet organizational index from 24% to 28.8%.

Overall, based on the similar β-sheet organizational indices and identical 1,530 cm^{-1} peak intensities, sulfo-SMCC-mediated cross-linking likely did not significantly alter the assembled β-sheet structures. Indeed, self-assembly is usually a fast process under standard conditions (final macroscopic hydrogelation may be a matter of a few seconds) [38, 49, 50], while sulfo-SMCC cross-linking could be much slower, from a few hours to one day (Fig. 3). Therefore, sulfo-SMCC may act as a molecular rope, cross-linking the pre-existing self-assembled CK structures without eliciting further secondary structure rearrangements.

3.4 X-ray characterization

In XRD analysis, the CK and crossCK peptides showed the presence of peaks at similar distances, with the exception of the peak at 0.6 nm (Fig. 4(c)). The 0.6 nm

spacing is related to the length of the lysine side-chain, whose signal in the crossCK was probably masked by linking with imide moieties.

The strong peak at 4.5 Å, ascribable to the spacing distance between peptide backbones in β-sheets [51], was almost unchanged between the two peptides.

Other similar peaks were observed at 3.27 Å (the distance between each residue along the peptide chain); 2 Å (the second order of the 4.5 Å peak); 2.4 nm (the thickness of a bilayered β-sheet structure, a typical structure found in similar self-assembling and co-assembling peptides [38, 52]); and 1.2 nm (the distance between the two layers of a double β-sheet structure). These similarities supported the hypothesis that the overall structure of the CK peptide was not perturbed by sulfo-SMCC cross-linking, thus further confirming the data obtained by ATR-FTIR.

Peaks at ~ 1.4, 0.6 nm, 1.9, and ~ 3 Å were also confirmed by WAXS analysis (Fig. 4(d)); the crossCK peptide displayed a significant enhancement in the highest peaks at ~ 3 and 1.9 Å, likely as a result of stronger backbone ordering after cross-linking. Modest peak shifts between XRD and WAXS data were ascribable to different sample preparations for the two techniques (see ESM for details).

Therefore, cross-linking presumably links multiple CK molecules and tightens up peptide backbone packing, without affecting assembled β-sheet structures. At higher scales, this phenomenon may cause the increased viscosity and stiffness detected by the rheology tests.

3.5 Morphological characterization

AFM morphological analysis was carried out to monitor the effects of cross-linking on the aggregation of CK into ordered nanostructures. Both the CK and crossCK peptides formed nanofibers (Fig. 5), with CK yielding short, single fibers typical of polyelectrolyte peptides [53, 54]. CK fibers were ~ 8–17 nm in width and ~ 0.8–1.8 nm in height (see ESM for details). Intriguingly, in the early stages of the cross-linking reaction (30 min), the crossCK peptides were paired and side-by-side packing of the fibers) was preferred. By contrast, at longer cross-linking reaction times, there was an increasing presence of flat clumped-fibers (2–6 h) (Figs. S5(a) and S5(b) in the ESM), which finally led to a tight and clustered network of presumably cross-linked nanofibers (24 h). Morphometrical analysis showed that crossCK fibers were ~ 30–52 nm in width and ~ 4–10 nm in height. Indeed, the width distributions of nanofibers of CK and crossCK were remarkably different at 6 h and 24 h of the cross-linking reaction (Fig. S5(c) in the ESM), as confirmed by fiber-width distribution analysis during the time course of the cross-linking reaction (Fig. S5(d) in the ESM). Furthermore, while CK showed the formation of individual fibers of 0.85 nm in height, analysis of crossCK heights showed a preponderance of heights of 5.4 nm, which suggested the piling up of multiple nanofibers.

From a morphological point of view, cross-linking did not hamper the CK's propensity to self-assemble, but, on the contrary, fostered a "clustering effect" of the self-assembled nanofibers, favoring their pairing at higher levels of hierarchical organization.

3.6 Molecular dynamics simulations

To verify some of the hypotheses drawn during the empirical characterization of CK and crossCK, and to evaluate the suitability of CK peptides to host cross-linked network formation, we ran CG molecular dynamics simulations of CK peptides (5%, w/v concentration) (see ESM for details). CG simulations were 3,000 ns long, a time frame that can be roughly scaled to a simulation time of 12 μs at an atomistic level [34]. Lysine side-chains were considered fully protonated at neutral pH, and Cl^- ions were added for neutralization. Initial conformations of peptides were fully extended; the secondary structure parameters used during simulations corresponded to extended and coil conformations for peptide backbones (LKLKLKLKLKLK) and side residues (CGG), respectively.

The extended structure was chosen because of the presence of equally spaced identical charges along the same short peptide chain, while random coil was preferred for the presence of the glycine spacer, which confers a high degree of conformational mobility [38]. Simulations showed a spontaneous organization of the extended peptides into bilayered blocks and a mutual orientation of adjacent strands comprising both parallel

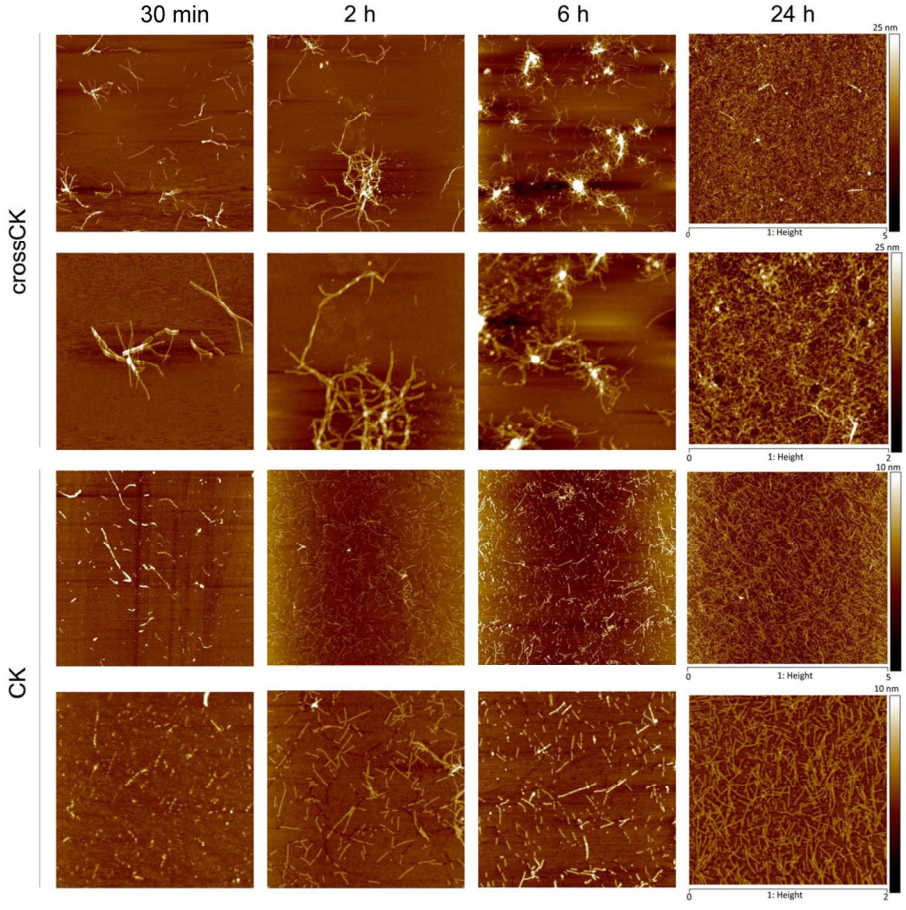

Figure 5 AFM morphological analysis at different time points. CK self-assembled into single short nanofibers, while crossCK self-organized into larger nanofibers. In the early stages of the cross-linking reaction (30 min), pairing and side-by-side packing of the nanofibers were promoted. 2–6 h after the start of the cross-linking reaction, there was a prevailing presence of flat entangled fibers, which finally led to a tight and clustered network of nanofibers (24 h). Fiber widths were ~8–17 nm and ~30–52 nm for CK and crossCK, respectively, while heights were ~0.8–1.8 nm and ~4–10 nm, respectively.

and anti-parallel β-sheets (Fig. 6(a)). Similar to CAPs and RADA16-like peptides [38, 52], leucine side-chains packed into a hydrophobic inner layer, while lysines were exposed to the solvent. In multiple bilayered blocks, each β-sheet was usually composed of 8–9 peptides. In other words, the assembly process started with the formation of small aggregates caused by hydrophobic patching, followed by a flattening of the layers shaped by the balance between hydrophobic collapse and same-charge repulsion. Notably, the blocks, whose edges were weakly interconnected, formed a reticulated arrangement that was still present at the end of the simulations. Repulsions between positively charged surfaces of the bilayered blocks likely prevented standard assembly into a single, larger aggregate; this, in turn, would allow for the consistent presence of multiple contact points among different protofibers formed by multiple bilayered blocks. The average detected contact distance of ~ 10 Å was compatible with the cross-linker spacer arm [55] and, therefore, with sulfo-SMCC-mediated cross-linking (Fig. 6(b)).

CG simulations of CK confirmed 0.45 nm as the main distance between peptide chains composing the β-sheets. The spacing distance between backbones belonging to opposite sheets of the bilayer was 1.2 nm, while the overall bilayer thickness (including peptide side-chains) was 2.4 nm. The 0.38 nm spacing was related to the distance between each residue along the chain. In addition, a spacing of 1.6 nm was assigned to the distance between two different paired bilayers (Fig. S6 in the ESM). All simulated data were in good agreement with the experimental data obtained through

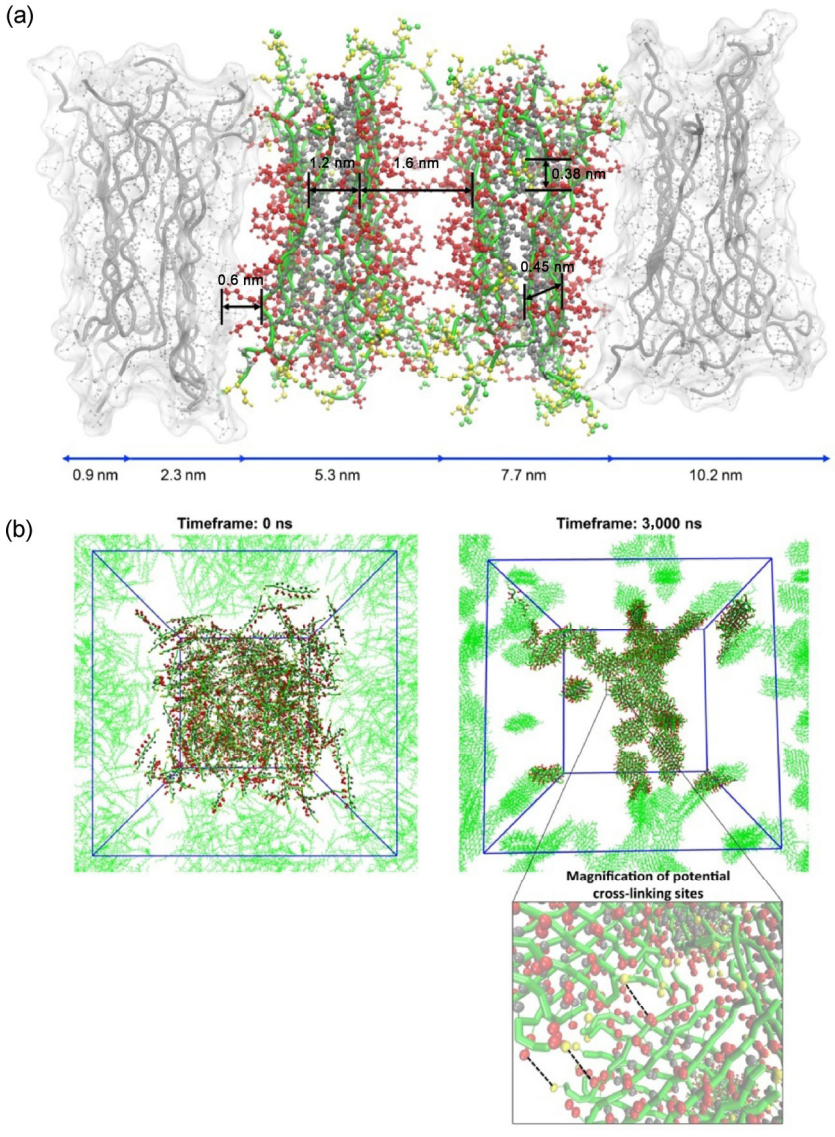

Figure 6 All-atom structure of self-aggregated blocks of the CK peptide back-mapped from CG molecular dynamic simulations. (a) To model a portion of a fiber, four replicas of the bilayer block are stacked in accordance with the mutual distances detected during CG simulations. In the two central blocks, the backbones are shown in green, while side-chains of leucine, lysine, glycine, and cysteine are shown in gray, red, white, and yellow, respectively. In self-aggregated structures of crossCK, the spacing distance between peptide backbones comprising the β-sheets is 0.45 nm. Spacing between β-sheets composing a bilayer is 1.2 nm, while two different paired bilayers could pile up at a distance of 1.6 nm (also see Fig. S6 in the ESM). Values at the bottom (blue lines beginning from the left end) show lengths extrapolated from piling of single and multiple bilayered β-sheets. Measurements from simulated data are in agreement with the previously described experimental data. (b) Initial and final configurations of the 300-peptide system of CK at t = 0 and t = 3,000 ns. Shown in green are system replicas useful to appreciate side-structuring. Initial random distribution of the peptides led to bilayered and entangled building blocks of β-sheets. Blocks formed irregular clusters in weak contact with each other, resulting into reticulated arrangements. The magnified field below shows the potential cross-linking sites between different blocks.

XRD and WAXS (Table S1 in the ESM), and, moreover, highlighted a collective spontaneous arrangement of the peptides in a network of β-structured bilayered patches, which could serve as a substrate for the cross-linking reaction. Lastly, CG simulation data and AFM analysis enabled us to propose a structural model in which the minimal exposure of hydrophobic groups to water and the formation of stable covalent bonds between different layers led to the piling of multiple bilayered β-sheets. Indeed, the sizes extrapolated from

simulation data (0.9 nm for a single layer; and 2.3, 5.3, 7.7, and 10.2 nm for the pairings of multiple layers of β-sheets) are in agreement with heights obtained through AFM analysis of crossCK. It should be noted that the molecular dynamics formation of cross-linked networks has mainly been documented for polymers [56], whereas in the peptides field, cross-linking has been used to investigate the nanomechanics of collagen [57] and to evaluate the effects of cross-linking on Aβ-oligomers [58]. In our case, the structures of the CK fibers were not available in the literature, and the modeling of cross-linked peptides would require an *ex vivo* parameterization endeavor to insert the cross-linker molecule before analyzing contacts between peptide molecules in molecular dynamics. Therefore, we investigated the likelihood of the formation of CK peptide oligomers (and of a cross-linked network) in systems with high concentrations of peptides, as a prerequisite for future modeling applications.

3.7 *In vitro* 2D cell cultures

To determine whether the standard good biocompatibility (and therefore potential for regenerative medicine applications) of the assembling peptide was affected by the cross-linking reaction, crossCK was tested in terms of viability and differentiation of hNSCs. hNSCs are a well-standardized source of somatic human nerve cells for *in vitro* testing of biomaterials [59], and have already been used in a cell therapy-based clinical trial because of their pro-regenerative potential [37]. hNSCs were seeded on the top surface of CK and crossCK, over plastic wells coated with Cultrex® substrate (positive control), and on untreated plastic wells (negative control, named Control) (see ESM).

The morphology of the differentiating hNSC progeny was examined after 7 days *in vitro* (7DIV). Cell anchoring and spreading is the first requirement to induce the differentiation and migration of hNSC in cell therapies, but it is also a favorable interaction of host-tissue nervous cells with implanted scaffolds *in vivo* [17]. hNSCs cultured on crossCK and Cultrex showed spread and branched cellular morphology, unlike the round clusters of cells found on Control (Fig. 7(a)).

Cell proliferation and viability were assessed via MTT assay (Fig. 7(a1)). The MTT assay revealed similar numbers of viable cells for crossCK (0.18 ± 0.023 a.u. (arbitrary units)) and Cultrex (0.172 ± 0.008 a.u.), while significantly lower values were detected on Control (0.064 ± 0.016 a.u.) compared with Cultrex (**$p < 0.01$) and crossCK ($^{§§}p < 0.01$).

hNSC progeny previously cultured for 7DIV were assayed for markers of different cell types; βIII-tubulin (neurons, in green), GFAP (astrocytes, in red), and GalC/O4 (oligodendrocytes, in red) (Fig. 7(b)) (See ESM for details). Single-channel images are shown in Fig. S7 in the ESM. Proportions of βIII-tubulin$^+$ cells were 24.3 ± 0.6% on Cultrex, 14.81 ± 4.93% on Control, 18.53 ± 0.88% on CK, and 13.96 ± 1.24% on the crossCK scaffold (Fig. 7(c)), with no relevant differences among the tested substrates. On the other hand, proportions of GFAP$^+$ cells were 39.11 ± 1.87%, 18.36 ± 3.28%, 32.11 ± 5.04%, and 21.87 ± 1.68% for Cultrex, Control, CK, and crossCK, respectively. On Control and crossCK, the percentages of GFAP$^+$ cells were significantly lower compared with Cultrex (***$p < 0.001$ and **$p < 0.01$, respectively). Proportions of GalC/O4$^+$ cells were 18.9 ± 1.98% on Cultrex, 10.01 ± 0.94% on Control, 14.29 ± 0.76% on CK, and 17.74 ± 0.94% on crossCK. Significant differences were found for Cultrex vs. Control (**$p < 0.01$) and crossCK vs. Control ($^{§}p < 0.05$). Because of the satisfactory cell viability and differentiation into the three main neuronal phenotypes on crossCK, we could assume that there was no cytotoxicity resulting from residues of the unreacted sulfo-SMCC; this is in agreement with previous findings from Raman spectroscopy data, suggesting total removal of unreacted sulfo-SMCC from the cross-linked scaffold before cell seeding.

In summary, viability, spreading, and differentiation tests of hNSCs on crossCK provided encouraging data similar to those obtained with ordinary non-functionalized SAPs seeded in 2D conditions [59], with an important difference; increments in storage modulus for crossCK seemed to be less effective in influencing NSC differentiation than expected from the literature. This was likely because the extensive cross-linking in crossCK altered the total net positive charge of the hydrogel, thereby partially counter-balancing the potential increase of GFAP$^+$ cells usually found in stiff substrates [20, 60, 61]. Indeed, as shown by the trinitrobenzenesulfonic acid (TNBSA) assay (see

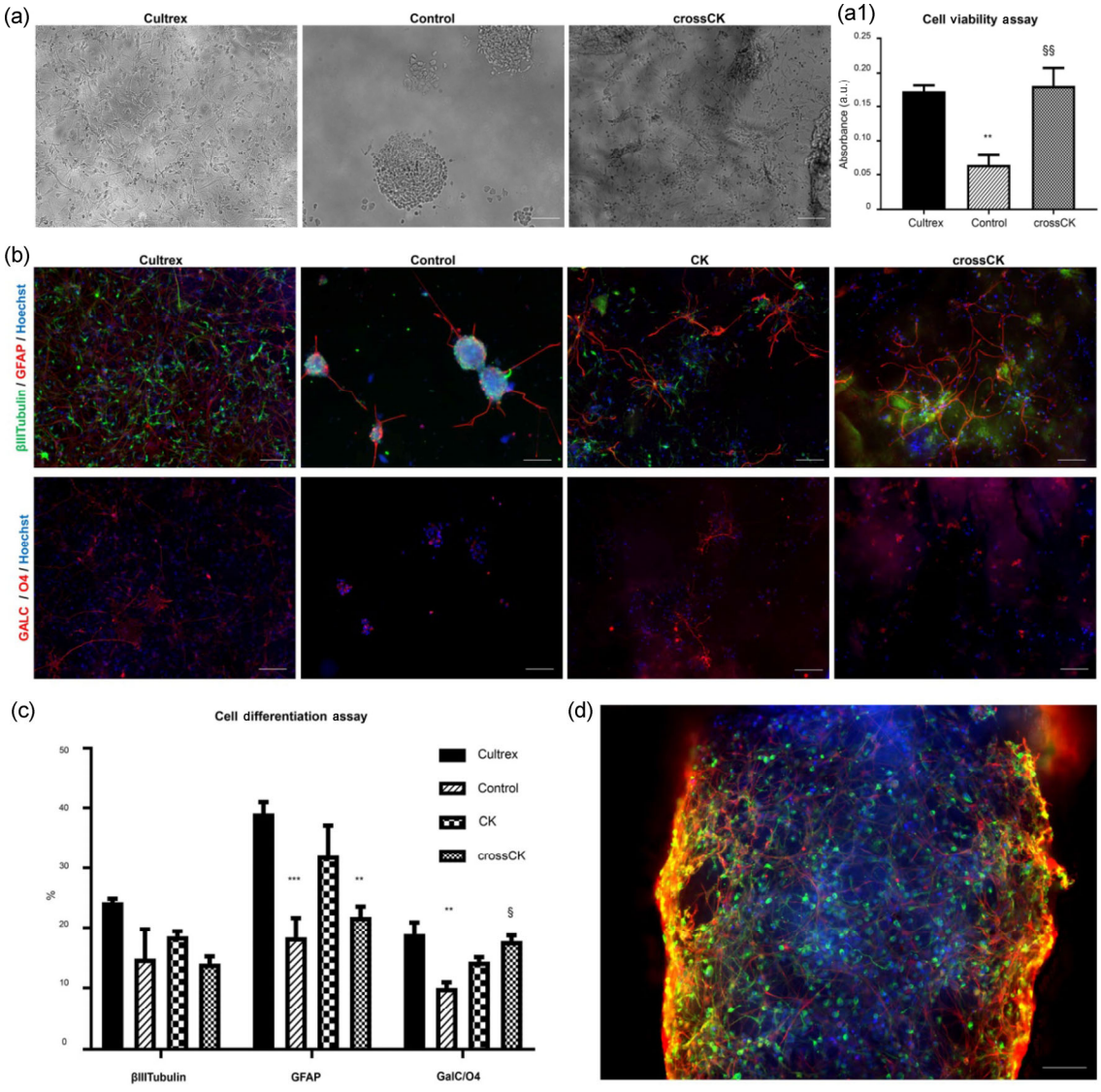

Figure 7 Viability and differentiation assays of hNSCs seeded on Cultrex, Control (plastic), CK, and crossCK. (a) Morphology and (a1) viability of hNSCs cultured for 7 DIV. No significant difference in cell spreading was detected between cells cultured on Cultrex and crossCK. The MTT assay assessing cell viability showed significant differences for Control vs. Cultrex (**$p < 0.01$) and Control vs. crossCK ($^{§§}p < 0.01$) ($n = 4$). No significant difference was found between Cultrex and crossCK. (b) Differentiation of hNSC (7DIV) into neurons (green), astrocytes (red), and oligodendrocytes (red) was performed with βIII-tubulin, GFAP, and GalC/O4, respectively. Cell nuclei were stained with Hoechst (blue). (c) Staining for the GFAP marker revealed significant differences in the case of Cultrex vs. Control (**$p < 0.001$) and Cultrex vs. crossCK (**$p < 0.01$); no significant difference was detected in the case of βIII-tubulin$^+$ cells ($n = 3$). The percentage of GalC/O4$^+$ cells was significantly higher for Cultrex (**$p < 0.01$) and crossCK ($^{§}p < 0.05$) compared with Control. (d) Immunofluorescence imaging of neurons (green) and astrocytes (red) inside a hollow crossCK microchannel (14DIV) showed the formation of a network of differentiating cells with branched morphology. No hypoxic effect for cells cultured into the inner lumens was identified. All scale bars are 100 μm.

ESM for details), the final outcome of the cross-linking reaction was a decrease in free primary amino groups down to ~ 76% of the initial value for CK (Fig. S8 in the ESM), likely as a result of their chemical linking with NHS-ester groups of sulfo-SMCC. This, in turn, presumably decreased (but not obliterated) the total net positive charges of crossCK.

Nonetheless, crossCK effects on stem cell differentiation can likely be ameliorated by introducing peptide functionalization, either as an additional functional

motif at one terminus, or as a functionalized co-assembling peptide (with opposite backbone net charge) to be matched to the already cross-linked networks of crossCK [20, 38].

Last, we tested the possibility of culturing NSCs in some of the obtained scaffolds pictured in Fig. 1. In particular, given that microchannel production is a crucial asset in neuro-regenerative therapies aiming to influence the spatial orientation of regenerating nervous fibers [17], special care was dedicated to the idea of injecting and culturing hNSCs in the hollow inner lumens, as depicted in Fig. 7(d). Inside the transparent crossCK channels, hNSC progeny showed spread and branched morphologies, with the presence of βIII-tubulin$^+$ and GFAP$^+$ cells after 14 days in culture, a significant step toward new solid scaffolds made entirely of biomimetic peptides.

4 Conclusions

SAPs feature the unquestionable asset of being designed at the molecular scale, allowing tunability for specific applications, but they have so far lacked the biomechanical properties required to be widely adopted in regenerative therapies other than those suited to soft materials [22].

The cross-linking strategy introduced and characterized here represents the previously missing link between tailorable and biomimetic self-assembling biomaterials and the processable scaffolds required to effectively target the regeneration of tissues such as skin, cornea, peripheral nerves, and small vessels. In addition, SAP cross-linking could potentially be adopted in electro-spinning, a promising technique minimally used with SAPs because of their intrinsic limited molecular weight and viscoelastic properties [62, 63]. Other unexpected applications may now be considered for future research beyond regenerative medicine.

Author contributions

R. P. and F. G. conceived the project. R. P. synthesized the peptides and carried out all experiments except for *in vitro* tests and molecular dynamics, which were conducted by A. M. and G. S. respectively. R. Z. co-supervised XRD, WAXS, and Raman experiments. R. P. and F. G. wrote the manuscript.

Acknowledgements

Work described and performed by R. P., G. S., and F. G. was funded by Fondazione Cariplo under Grant no. 2011-0352, by La Colonna Onlus, by the "Ricerca Corrente 2015-2016" funding granted by the Italian Ministry of Health and by the "5 x 1000" voluntary contributions. A. M. is supported by a fellowship granted by Vertical Onlus. Raman, XRD, FTIR and WAXS experiments were conducted at the Advanced Light Source and at the Molecular Foundry, at the Lawrence Berkeley National Laboratory, both of which are supported by the Office of Science, under Contract No. DE-AC02-05CH11231. We thank Alice Nodari for her help in SAP production and QC tests.

Electronic Supplementary Material: Supplementary material is available in the online version of this article at http://doi.org/10.1007/s12274-017-1834-6.

References

[1] Matson, J. B.; Stupp, S. I. Self-assembling peptide scaffolds for regenerative medicine. *Chem. Commun.* **2012**, *48*, 26–33.

[2] Saracino, G. A. A.; Cigognini, D.; Silva, D.; Caprini, A.; Gelain, F. Nanomaterials design and tests for neural tissue engineering. *Chem. Soc. Rev.* **2013**, *42*, 225–262.

[3] Morgan, C. E.; Dombrowski, A. W.; Rubert Pérez, C. M.; Bahnson, E. S. M.; Tsihlis, N. D.; Jiang, W. L.; Jiang, Q.; Vercammen, J. M.; Prakash, V. S.; Pritts, T. A. et al. Tissue-factor targeted peptide amphiphile nanofibers as an injectable therapy to control hemorrhage. *ACS Nano* **2016**, *10*, 899–909.

[4] Ozeki, M.; Kuroda, S.; Kon, K.; Kasugai, S. Differentiation of bone marrow stromal cells into osteoblasts in a self-assembling peptide hydrogel: *In vitro* and *in vivo* studies. *J. Biomater. Appl.* **2011**, *25*, 663–684.

[5] Schneider, A.; Garlick, J. A.; Egles, C. Self-assembling peptide nanofiber scaffolds accelerate wound healing. *PLoS One* **2008**, *3*, e1410.

[6] Loo, Y.; Wong, Y. C.; Cai, E. Z.; Ang, C. H.; Raju, A.; Lakshmanan, A.; Koh, A. G.; Zhou, H. J.; Lim, T. C.; Moochhala, S. M. et al. Ultrashort peptide nanofibrous hydrogels for the acceleration of healing of burn wounds. *Biomaterials* **2014**, *35*, 4805–4814.

[7] Tysseling-Mattiace, V. M.; Sahni, V.; Niece, K. L.; Birch, D.; Czeisler, C.; Fehlings, M. G.; Stupp, S. I.; Kessler, J. A. Self-assembling nanofibers inhibit glial scar formation and promote axon elongation after spinal cord injury. *J. Neurosci.* **2008**, *28*, 3814–3823.

[8] Yan, C. Q.; Pochan, D. J. Rheological properties of peptide-based hydrogels for biomedical and other applications. *Chem. Soc. Rev.* **2010**, *39*, 3528–3540.

[9] Davis, M. E.; Michael Motion, J. P.; Narmoneva, D. A.; Takahashi, T.; Hakuno, D.; Kamm, R. D.; Zhang, S.; Lee, R. T. Injectable self-assembling peptide nanofibers create intramyocardial microenvironments for endothelial cells. *Circulation* **2005**, *111*, 442–450.

[10] Cigognini, D.; Silva, D.; Paloppi, S.; Gelain, F. Evaluation of mechanical properties and therapeutic effect of injectable self-assembling hydrogels for spinal cord injury. *J. Biomed. Nanotechnol.* **2014**, *10*, 309–323.

[11] Tao, H.; Wu, Y. H.; Li, H. F.; Wang, C. F.; Zhang, Y.; Li, C.; Wen, T. Y.; Wang, X. M.; He, Q.; Wang, D. L. et al. BMP7-based functionalized self-assembling peptides for nucleus pulposus tissue engineering. *ACS Appl. Mater. Interfaces* **2015**, *7*, 17076–17087.

[12] Tatman, P. D.; Gerull, W.; Sweeney-Easter, S.; Davis, J. I.; Gee, A. O.; Kim, D. H. Multiscale biofabrication of articular cartilage: Bioinspired and biomimetic approaches. *Tissue Eng. B Rev.* **2015**, *21*, 543–559.

[13] Brunton, P. A.; Davies, R. P.; Burke, J. L.; Smith, A.; Aggeli, A.; Brookes, S. J.; Kirkham, J. Treatment of early caries lesions using biomimetic self-assembling peptides--A clinical safety trial. *Br. Dent. J.* **2013**, *215*, E6.

[14] Sang, L. Y. H.; Liang, Y. X.; Li, Y.; Wong, W. M.; Tay, D. K. C.; So, K. F.; Ellis-Behnke, R. G.; Wu, W. T.; Cheung, R. T. F. A self-assembling nanomaterial reduces acute brain injury and enhances functional recovery in a rat model of intracerebral hemorrhage. *Nanomed.: Nanotechnol. Biol. Med.* **2015**, *11*, 611–620.

[15] Guo, J. S.; Leung, K. K.; Su, H. X.; Yuan, Q. J.; Wang, L.; Chu, T. H.; Zhang, W. M.; Pu, J. K. S.; Ng, G. K. P.; Wong, W. M. et al. Self-assembling peptide nanofiber scaffold promotes the reconstruction of acutely injured brain. *Nanomed.: Nanotechnol. Biol. Med.* **2009**, *5*, 345–351.

[16] Cigognini, D.; Satta, A.; Colleoni, B.; Silva, D.; Donegà, M.; Antonini, S.; Gelain, F. Evaluation of early and late effects into the acute spinal cord injury of an injectable functionalized self-assembling scaffold. *PLoS One* **2011**, *6*, e19782.

[17] Gelain, F.; Panseri, S.; Antonini, S.; Cunha, C.; Donega, M.; Lowery, J.; Taraballi, F.; Cerri, G.; Montagna, M.; Baldissera, F. et al. Transplantation of nanostructured composite scaffolds results in the regeneration of chronically injured spinal cords. *ACS Nano* **2011**, *5*, 227–236.

[18] Yang, H. N.; Yang, H. L.; Xie, Z. H.; Wang, P.; Bi, J. Z. Self-assembling nanofibers alter the processing of amyloid precursor protein in a transgenic mouse model of Alzheimer's disease. *Neurol. Res.* **2015**, *37*, 84–91.

[19] Xiong, N.; Dong, X. Y.; Zheng, J.; Liu, F. F.; Sun, Y. Design of lvffark and lvffark-functionalized nanoparticles for inhibiting amyloid β-protein fibrillation and cytotoxicity. *ACS Appl. Mater. Interfaces* **2015**, *7*, 5650–5662.

[20] Caprini, A.; Silva, D.; Zanoni, I.; Cunha, C.; Volontè, C.; Vescovi, A.; Gelain, F. A novel bioactive peptide: Assessing its activity over murine neural stem cells and its potential for neural tissue engineering. *N. Biotechnol.* **2013**, *30*, 552–562.

[21] Gelain, F.; Unsworth, L. D.; Zhang, S. G. Slow and sustained release of active cytokines from self-assembling peptide scaffolds. *J. Control. Rel.* **2010**, *145*, 231–239.

[22] Pugliese, R.; Gelain, F. Peptidic biomaterials: From self-assembling to regenerative medicine. *Trends Biotechnol.* **2016**, *35*, 145–158.

[23] Kasoju, N.; Bora, U. Silk fibroin in tissue engineering. *Adv. Healthcare Mater.* **2012**, *1*, 393–412.

[24] Ibusuki, S.; Halbesma, G. J.; Randolph, M. A.; Redmond, R. W.; Kochevar, I. E.; Gill, T. J. Photochemically cross-linked collagen gels as three-dimensional scaffolds for tissue engineering. *Tissue Eng.* **2007**, *13*, 1995–2001.

[25] Ma, L.; Gao, C. Y.; Mao, Z. W.; Zhou, J.; Shen, J. C.; Hu, X. Q.; Han, C. M. Collagen/chitosan porous scaffolds with improved biostability for skin tissue engineering. *Biomaterials* **2003**, *24*, 4833–4841.

[26] Olofsson, C.; Ahl, T.; Johansson, T.; Larsson, S.; Nellgård, P.; Ponzer, S.; Fagrell, B.; Przybelski, R.; Keipert, P.; Winslow, N. et al. A multicenter clinical study of the safety and activity of maleimide-polyethylene glycol-modified hemoglobin (hemospan®) in patients undergoing major orthopedic surgery. *Anesthesiology* **2006**, *105*, 1153–1163.

[27] Gilewski, T.; Ragupathi, G.; Bhuta, S.; Williams, L. J.; Musselli, C.; Zhang, X. F.; Bornmann, W. G.; Spassova, M.; Bencsath, K. P.; Panageas, K. S. et al. Immunization of metastatic breast cancer patients with a fully synthetic globo H conjugate: A phase I trial. *Proc. Natl. Acad. Sci. USA* **2001**, *98*, 3270–3275.

[28] Björkholm, M.; Fagrell, B.; Przybelski, R.; Winslow, N.; Young, M.; Winslow, R. M. A phase I single blind clinical trial of a new oxygen transport agent (MP4), human hemoglobin modified with maleimide-activated polyethylene glycol. *Haematologica* **2005**, *90*, 505–515.

[29] Riddles, P. W.; Blakeley, R. L.; Zerner, B. Reassessment of Ellman's reagent. *Methods Enzymol.* **1983**, *91*, 49–60.

[30] Riddles, P. W.; Blakeley, R. L.; Zerner, B. Ellman's reagent: 5,5'-dithiobis(2-nitrobenzoic acid)--a reexamination. *Anal. Biochem.* **1979**, *94*, 75–81.

[31] Gelain, F.; Silva, D.; Caprini, A.; Taraballi, F.; Natalello, A.; Villa, O.; Nam, K. T.; Zuckermann, R. N.; Doglia, S. M.; Vescovi, A. Bmhp1-derived self-assembling peptides: Hierarchically assembled structures with self-healing propensity and potential for tissue engineering applications. *ACS Nano* **2011**, *5*, 1845–1859.

[32] Hexemer, A.; Bras, W.; Glossinger, J.; Schaible, E.; Gann, E.; Kirian, R.; MacDowell, A.; Church, M.; Rude, B.; Padmore, H. A SAXS/WAXS/GISAXS beamline with multilayer monochromator. *J. Phys.: Conf. Ser.* **2010**, *247*, 012007.

[33] Taraballi, F.; Campione, M.; Sassella, A.; Vescovi, A.; Paleari, A.; Hwang, W.; Gelain, F. Effect of functionalization on the self-assembling propensity of β-sheet forming peptides. *Soft Matter* **2009**, *5*, 660–668.

[34] Marrink, S. J.; Risselada, H. J.; Yefimov, S.; Tieleman, D. P.; de Vries, A. H. The MARTINI force field: Coarse grained model for biomolecular simulations. *J. Phys. Chem. B* **2007**, *111*, 7812–7824.

[35] Monticelli, L.; Kandasamy, S. K.; Periole, X.; Larson, R. G.; Tieleman, D. P.; Marrink, S. J. The martini coarse-grained force field: Extension to proteins. *J. Chem. Theory Comput.* **2008**, *4*, 819–834.

[36] Van Der Spoel, D.; Lindahl, E.; Hess, B.; Groenhof, G.; Mark, A. E.; Berendsen, H. J. C. Gromacs: Fast, flexible, and free. *J. Comput. Chem.* **2005**, *26*, 1701–1718.

[37] Mazzini, L.; Gelati, M.; Profico, D. C.; Sgaravizzi, G.; Projetti Pensi, M.; Muzi, G.; Ricciolini, C.; Rota Nodari, L.; Carletti, S.; Giorgi, C. et al. Human neural stem cell transplantation in als: Initial results from a phase i trial. *J. Transl. Med.* **2015**, *13*, 17.

[38] Raspa, A.; Saracino, G. A. A.; Pugliese, R.; Silva, D.; Cigognini, D.; Vescovi, A.; Gelain, F. Complementary co-assembling peptides: From *in silico* studies to *in vivo* application. *Adv. Funct. Mater.* **2014**, *24*, 6317–6328.

[39] Zhang, S. G. Fabrication of novel biomaterials through molecular self-assembly. *Nat. Biotechnol.* **2003**, *21*, 1171–1178.

[40] Haines-Butterick, L.; Rajagopal, K.; Branco, M.; Salick, D.; Rughani, R.; Pilarz, M.; Lamm, M. S.; Pochan, D. J.; Schneider, J. P. Controlling hydrogelation kinetics by peptide design for three-dimensional encapsulation and injectable delivery of cells. *Proc. Natl. Acad. Sci. USA* **2007**, *104*, 7791–7796.

[41] Ding, Y.; Li, Y.; Qin, M.; Cao, Y.; Wang, W. Photo-cross-linking approach to engineering small tyrosine-containing peptide hydrogels with enhanced mechanical stability. *Langmuir* **2013**, *29*, 13299–13306.

[42] Khalily, M. A.; Goktas, M.; Guler, M. O. Tuning viscoelastic properties of supramolecular peptide gels via dynamic covalent crosslinking. *Org. Biomol. Chem.* **2015**, *13*, 1983–1987.

[43] Riener, C. K.; Kada, G.; Gruber, H. J. Quick measurement of protein sulfhydryls with Ellman's reagent and with 4,4'-dithiodipyridine. *Anal. Bioanal. Chem.* **2002**, *373*, 266–276.

[44] Maiti, N. C.; Apetri, M. M.; Zagorski, M. G.; Carey, P. R.; Anderson, V. E. Raman spectroscopic characterization of secondary structure in natively unfolded proteins: α-synuclein. *J. Am. Chem. Soc.* **2004**, *126*, 2399–2408.

[45] Jain, R.; Agarwal, A.; Kierski, P. R.; Schurr, M. J.; Murphy, C. J.; McAnulty, J. F.; Abbott, N. L. The use of native chemical functional groups presented by wound beds for the covalent attachment of polymeric microcarriers of bioactive factors. *Biomaterials* **2013**, *34*, 340–352.

[46] Schagger, H. Tricine-SDS-PAGE. *Nat. Protoc.* **2006**, *1*, 16–22.

[47] Chirgadze, Y. N.; Nevskaya, N. A. Infrared spectra and resonance interaction of amide-i vibration of the antiparallel-chain pleated sheet. *Biopolymers* **1976**, *15*, 607–625.

[48] Sarroukh, R.; Goormaghtigh, E.; Ruysschaert, J. M.; Raussens, V. ATR-FTIR: A "rejuvenated" tool to investigate amyloid proteins. *Biochim. Biophys. Acta* **2013**, *1828*, 2328–2338.

[49] Hwang, W.; Zhang, S.; Kamm, R. D.; Karplus, M. Kinetic control of dimer structure formation in amyloid fibrillogenesis. *Proc. Natl. Acad. Sci. USA* **2004**, *101*, 12916–12921.

[50] Saracino, G. A. A.; Gelain, F. Modelling and analysis of early aggregation events of bmhp1-derived self-assembling peptides. *J. Biomol. Struct. Dyn.* **2014**, *32*, 759–775.

[51] Sunde, M.; Serpell, L. C.; Bartlam, M.; Fraser, P. E.; Pepys, M. B.; Blake, C. C. F. Common core structure of amyloid fibrils by synchrotron X-ray diffraction. *J. Mol. Biol.* **1997**, *273*, 729–739.

[52] Yokoi, H.; Kinoshita, T.; Zhang, S. Dynamic reassembly of peptide rada16 nanofiber scaffold. *Proc. Natl. Acad. Sci. USA* **2005**, *102*, 8414–8419.

[53] Haynie, D. T. Physics of polypeptide multilayer films. *J. Biomed. Mater. Res. B: Appl. Biomater.* **2006**, *78B*, 243–252.

[54] Mermut, O.; Phillips, D. C.; York, R. L.; McCrea, K. R.; Ward, R. S.; Somorjai, G. A. *In situ* adsorption studies of a 14-amino acid leucine-lysine peptide onto hydrophobic polystyrene and hydrophilic silica surfaces using quartz crystal microbalance, atomic force microscopy, and sum frequency generation vibrational spectroscopy. *J. Am. Chem. Soc.* **2006**, *128*, 3598–3607.

[55] Hermanson, G. T. *Bioconjugate Techniques*; 3rd ed. Elsevier: Amsterdam, 2013.

[56] Demir, B.; Walsh, T. R. A robust and reproducible procedure for cross-linking thermoset polymers using molecular simulation. *Soft Matter* **2016**, *12*, 2453–2464.

[57] Buehler, M. J. Nanomechanics of collagen fibrils under varying cross-link densities: Atomistic and continuum studies. *J. Mech. Behav. Biomed. Mater.* **2008**, *1*, 59–67.

[58] Zhang, S. T.; Fox, D. M.; Urbanc, B. Insights into formation and structure of aβ oligomers cross-linked via tyrosines. *J. Phys. Chem. B* **2017**, *121*, 5523–5535.

[59] Gelain, F.; Bottai, D.; Vescovi, A.; Zhang, S. G. Designer self-assembling peptide nanofiber scaffolds for adult mouse neural stem cell 3-dimensional cultures. *PLoS One* **2006**, *1*, e119.

[60] Lee, J. H.; Jung, H. W.; Kang, I. K.; Lee, H. B. Cell behaviour on polymer surfaces with different functional groups. *Biomaterials* **1994**, *15*, 705–711.

[61] Cai, L.; Lu, J.; Sheen, V.; Wang, S. F. Optimal poly(L-lysine) grafting density in hydrogels for promoting neural progenitor cell functions. *Biomacromolecules* **2012**, *13*, 1663–1674.

[62] Tayi, A. S.; Pashuck, E. T.; Newcomb, C. J.; McClendon, M. T.; Stupp, S. I. Electrospinning bioactive supramolecular polymers from water. *Biomacromolecules* **2014**, *15*, 1323–1327.

[63] Singh, G.; Bittner, A. M.; Loscher, S.; Malinowski, N.; Kern, K. Electrospinning of diphenylalanine nanotubes. *Adv. Mater.* **2008**, *20*, 2332–2336.